JOURNAL OF GEOPHYSICAL RESEARCH: OCEANS, VOL. 118, 7117–7131, doi:10.1002/2013JC009158, 2013

Ice shelf/ocean interactions under the Amery Ice Shelf: Seasonal variability and its effect on marine ice formation

Laura Herraiz-Borreguero,[1] Ian Allison,[1] Mike Craven,[1,2] Keith W. Nicholls,[3] and Mark A. Rosenberg[1]

Received 28 May 2013; revised 28 October 2013; accepted 3 December 2013; published 26 December 2013.

[1] Marine ice is an important factor in ice shelf stability. An extensive marine ice layer is present under the Amery Ice Shelf (AIS), East Antarctica. This paper documents observations on the seasonal variability of the AIS-ocean interaction beneath the marine ice layer. We focus on data collected during 2002 through a borehole at AM01, 100 km from the ice shelf calving front, and use additional data from two other boreholes to complement the study. At AM01, the top ~20 m of the water column is super-cooled almost year round, protecting the marine ice layer and promoting frazil ice formation. The mixed layer thickness varies from ~50 m in February to at least 160 m by June, as the water column cools and freshens. High Salinity Shelf Water (HSSW) abruptly arrives at AM01 in June–August as an eddy-like flow. We suggest that the flow characteristics are a result of baroclinic instabilities. In addition, the inflow of HSSW results in a steepening of the isopycnals that enhances the upwelling of Ice Shelf Water. This study documents, for the first time, a seasonal signal in the formation of marine ice under the AIS. Our results highlight the vulnerability of the marine ice layer to ocean variability with potential consequences for the overall ice shelf mass balance.

Citation: Herraiz-Borreguero, L., I. Allison, M. Craven, K. W. Nicholls, and M. A. Rosenberg (2013), Ice shelf/ocean interactions under the Amery Ice Shelf: Seasonal variability and its effect on marine ice formation, *J. Geophys. Res. Oceans*, *118*, 7117–7131, doi:10.1002/2013JC009158.

1. Introduction

[2] Ice shelves are coastal areas of floating ice that extend from an ice sheet out over the ocean. Around Antarctica, ice shelves are the primary regions where the ice sheet discharges into the Southern Ocean. The mass budget of an ice shelf is the balance between ice inputs due to drainage from the grounded ice sheet (usually via fast-moving ice streams) local snow accumulation and basal refreezing; and ice loss from calving of icebergs at the ice front and basal melting. The basal melting of ice shelves is particularly sensitive to oceanic heat flux, an increase in which is thought to have led to a loss of Antarctic Ice Sheet mass [*Pritchard et al*., 2012]. This loss, which contributes to sea-level rise, is thought to be enhanced by the reduction in the buttress effect ice shelves have on the upstream ice sheet as a result of melt-induced thinning [*Scambos et al*., 2004]. A notable example of this is the observed thinning of the Pine Island Glacier ice shelf and what is considered to be a resulting increase in ice discharge to the Amundsen Sea, especially in recent years [e.g., *Jacobs et al*., 2011].

[3] Two processes define the ocean circulation underneath ice shelves in cold oceanographic regimes. The first process or *ice pump* is driven by the change in seawater freezing point with pressure [*Foldvik and Kvinge*, 1974], which will melt ice at depth and deposit ice at shallower depths to form a marine ice layer. It is self-starting [*Lewis and Perkins*, 1986]. The second process consists of an open circulation driven by the inflow of continental shelf waters, which causes ice shelf basal melt, and can potentially also contribute to the basal deposition of marine ice. In addition, a new water mass, Ice Shelf Water (ISW), is formed via both processes.

[4] ISW has a temperature below the surface freezing point and can form when the ambient ocean drives melting at the base of an ice shelf at typically several hundred meters depth. The excess buoyancy of the ISW due to the meltwater component causes it to ascend the upward-sloping base of the ice shelf. As ISW rises, its temperature might be exceeded by the in situ freezing point, which is also rising due to the reducing pressure. This can result in the formation of frazil ice crystals, which can accrete at the ice shelf base and form a layer of marine ice.

[5] High Salinity Shelf Water (HSSW) and Circumpolar Deep Water (CDW) are the two main water masses driving basal melting of ice shelves. HSSW is a by-product of sea-ice formation and is the densest water mass on the

[1]Antarctic Climate and Ecosystem Cooperative Research Centre, University of Tasmania, Hobart, Tasmania, Australia.
[2]Australian Antarctic Division, Channel Highway, Kingston, Tasmania, Australia.
[3]British Antarctic Survey, Cambridge, UK.

Corresponding author: L. Herraiz-Borreguero, Antarctic Climate and Ecosystem Cooperative Research Centre/University of Tasmania, Private Bag 80, Hobart, TAS 7001, Australia. (laurahebo@gmail.com)

2169-9275/13/10.1002/2013JC009158

Antarctic continental shelf. It has a temperature at, or close to, the surface freezing point and a wide range of salinity values [*Whitworth et al*., 1998]. Under Filchner-Ronne Ice Shelf, HSSW drives basal melt rates of up to 14 ± 2 m/yr [*Rignot and Jacobs*, 2002]. CDW upwells at the Antarctic continental slope and in some areas can cross the shelf break and reach ice shelves. Under the Pine Island Glacier ice shelf, CDW drives melt rates of up to 44 ± 6 m/yr [*Rignot and Jacobs*, 2002].

[6] In East Antarctica, the Lambert Glacier-Amery Ice Shelf system has long been a focus of Australian Antarctic research [e.g., *Budd*, 1966; *Morgan*, 1972; *Morgan and Budd*, 1975; *Allison*, 1979; *Budd et al*., 1982]. The Amery Ice Shelf (AIS), with an area of ~62,000 km^2, is the third largest embayed ice shelf in Antarctica and the largest wholly in East Antarctica (Figure 1). Although small compared with the Ross and the Filchner-Ronne ice shelves, the AIS is fed by the Lambert Glacier system, which drains ~16% of the area of East Antarctica [*Allison*, 1979]. The deepest part of the southern grounding line of the AIS is ~2500 m below sea level [*Fricker et al*., 2002] where there are very high basal melt rates. Around 25% of the melt is thought to refreeze as marine ice [*Wen et al*., 2010; *Galton-Fenzi et al*., 2012].

[7] The circulation in Prydz Bay consists of a large cyclonic gyre, centered in a deep channel [*Nunes Vaz and Lennon*, 1996; *Smith et al*., 1984]. The gyre is associated with a relatively narrow coastal current that runs along the Amery Ice Shelf calving front, and continues westward after leaving the Bay (Figure 1). Here the current becomes very strong, with currents along the western side of Prydz Bay exceeding 1 m s^{-1} [*Nunes Vaz and Lennon*, 1996].

[8] The marine ice layer under the Amery Ice Shelf is an important feature in the overall structure of the AIS. Up to 190 m thick, it accounts for ~9% of the ice-shelf's volume [*Fricker et al*., 2001]. It is found in the north-western sector of the AIS and extends all the way to the calving front [*Fricker et al*., 2001]. The thickest marine ice occurs in two longitudinal bands between the ice flow lines emanating from the Charybdis/Scylla Glacier and a flow trace from Jetty Peninsula. *Fricker et al*. [2001] also showed that the marine ice found at the base of the AIS preferentially forms in troughs. These troughs occur at the boundary between flow lines from the two adjacent ice streams feeding into the AIS (Figure 1) and an unnamed ice stream north of Single Island where they merge.

[9] Over the past decade, monitoring of the ocean underneath the Amery Ice Shelf has been an important objective of the Amery Ice Shelf-Ocean Research (AMISOR) Project. While significant data sets have been retrieved from beneath ice shelves in West Antarctica [*Clough and Hansen*, 1979; *Foster*, 1983; *Jacobs et al*., 1979; *Nicholls and Jenkins*, 1993], the AMISOR Project (2001-2012) is perhaps the most comprehensive study to date of ice shelf-ocean interactions. The AMISOR Project has made rare measurements from what is logistically an exceptionally challenging part of the cryosphere. A total of six instrumented moorings were deployed through hot water-drilled boreholes, three of them under the marine ice layer at sites AM01, AM04, and AM05 (Figure 1).

[10] This paper documents the seasonal cycle in ocean temperature and salinity at borehole site AM01, and gives new insights into the variability in the formation of the observed marine ice layer. Data collected at two different sites, AM04 and AM05, and from conventional moorings at the front of the Amery Ice Shelf, are used to complement the description of the ice-ocean interaction at site AM01. The complete AM01 data set spans 6 years (2002–2007). However, this paper focuses mostly on the temperature and salinity record from 2002, the only full year for which all three instruments at AM01 measured ocean temperature and salinity. The seasonal variability is described in general terms in section 4.3 for the entire 6 year record.

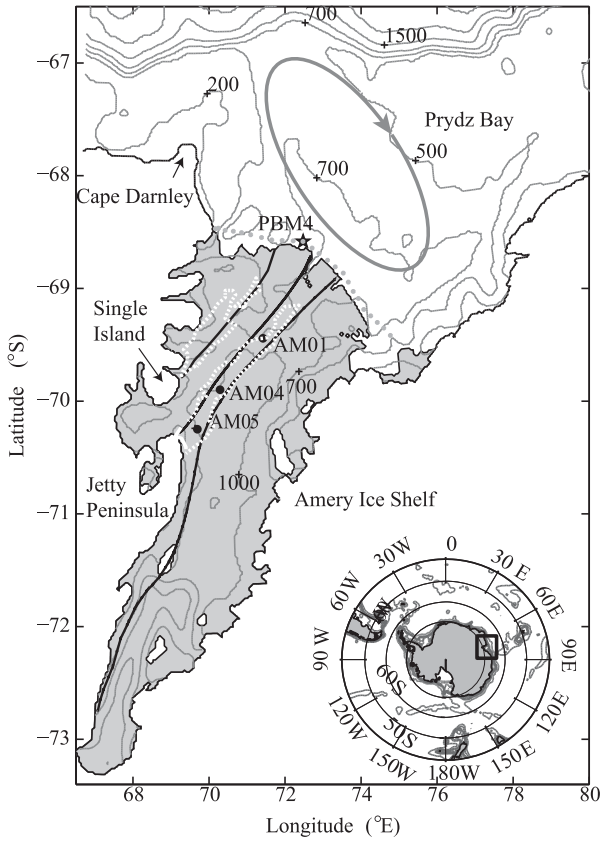

Figure 1. Amery Ice Shelf (dark gray) with borehole sites AM01, AM04, and AM05 (black dots). The PBM4 mooring at the front of the ice shelf is shown as a star, and ship hydrographic sections are shown as gray dots along the ice shelf front. The black thick lines are, from east to west, the Fisher Glacier and the Charybdis/Scylla Glacier flow lines [*Raup et al*., 2005]. Marine ice band of thickness larger than 100 m is shown by the white dashed contours. The Prydz Bay gyre is shown in gray. Bathymetry is shown as light gray contours (cavity bathymetry from *Galton-Fenzi et al*. [2008]).

2. Data

2.1. Borehole Survey

[11] As part of the AMISOR Project, three boreholes were hot water-drilled at AM01, AM04, and AM05, respectively, during the austral summers of 2001/2002, 2005/2006, and 2010/2011. Tables 1 and 2 provide information on the ice shelf physical characteristics and the instrument

Table 1. Amery Ice Shelf Characteristics at Borehole Sites AM01, AM04, and AM05[a]

Sites	Total Ice Shelf Thickness (m)	Marine Ice Layer Thickness (m)	Ice Shelf Elevation (m)	Ice Shelf Base (dbar)	Water Column Thickness (dbar)	Bottom Pressure (dbar)
AM01	479	100 (consolidated) 103 (permeable)	56	427	366	793
AM04	603	135 (consolidated) 70 (permeable)	64	533	417	950
AM05	624	~200	~70	560	360	920

[a]All pressure values are referenced to the mean sea surface; ice shelf elevation = distance from ice shelf surface to mean sea surface at the time of the borehole opening; bottom pressure = pressure at the bottom of the water column from the sea surface.

deployments at all three sites. These sites are within a marine ice band that extends approximately 250 km from the vicinity of Jetty Peninsula to the centre of the ice front. For details of the field operations and the hot water drill see *Craven et al*. [2004].

2.1.1. Borehole Site AM01

[12] Site AM01 (69.443°S, 71.418°E) is located approximately 100 km from the calving front of the AIS (Figure 1). At this site, the ice shelf is 479 m thick, of which the deepest 203 m is accreted marine ice [*Morgan*, 1972; *Craven et al*., 2004, 2009]. Two layers are distinguishable within the marine ice itself: a 100 m thick consolidated layer and a 103 m thick permeable layer. *Craven et al*. [2009] estimated an average marine ice accretion rate of 1.1 ± 0.2 m yr^{-1} along a flow line extending 80 km to the south of AM01. This suggests that, when taking into account strain thinning, nearly half of the marine ice layer present at AM01 is accreted downstream of AM04 [*Craven et al*., 2009].

2.1.2. Borehole Site AM04

[13] Borehole AM04 (69.901°S, 70.291°E) was drilled on the same flow line as AM01 and is approximately 170 km from the calving front (Figure 1). At AM04, the ice shelf is 603 m thick, of which the deepest 208 m is accreted marine ice. As at site AM01, the marine ice occurs in two layers, consisting of a 135 m thick consolidated layer and a 70 m thick permeable layer [*Craven et al*., 2009].

2.1.3. Borehole Site AM05

[14] Borehole AM05 (70.2293°S, 69.6805°E) was drilled on the same flow line as AM01 and AM04 and is approximately 210 km from the calving front (Figure 1). At AM05, the ice shelf is 624 m thick, of which the deepest 200 m is accreted marine ice.

2.2. Data Collection From the Ice Shelf Cavity

2.2.1. Conductivity-Temperature-Depth (CTD) Profiles

[15] Immediately after the hot water drilling and before the deployment of the mooring at site AM01, a series of CTD profiles were obtained from the ocean water column using a Falmouth Scientific (FSI) 3" microCTD (serial 1610). Prior to deployment, the FSI microCTD was compared against a General Oceanics Mark III CTD serial 1193 during an oceanographic cruise in Prydz Bay in February 2002 (Figure 1, gray dots). The FSI accuracies were estimated to be: temperature < 0.005°C, salinity < 0.004, and pressure ~2 dbar. Seven profiles were successfully retrieved from the AM01 site within the space of 4 days (Figure 2). These profiles give information about water column stratification during the austral summer and aid interpretation of the changes in potential temperature (θ) and salinity (S) observed in the sub-ice shelf mooring data (see below). Information on the data processing and calibration is given in Appendix A.

2.2.2. Subice Shelf Moorings

[16] At both sites, after CTD profiling, a mooring was deployed through the ice shelf into the ocean cavity. The moorings consisted of three *Seabird* 37IM Microcats (fixed at different depths) measuring temperature, salinity, and pressure at 30 min intervals. Manufacturer-supplied calibrations were applied internally by the Microcats, and calibrated data were output, with initial accuracies of 0.002°C for temperature, 0.003 (PSS78) for salinity, and 2 dbar for pressure. Table 2 summarizes the instrument deployments and the data retrieved. The depths were chosen to be within ~20 m of the ice shelf base, in the middle of the water column and within 20–50 m of the bottom of the water

Table 2. Details of Mooring Deployments Within the Water Column at Sites AM01, AM04, and AM05[a]

Sites	Deployment Date	Mean Deployed Pressure (dbar)	Measurements 1st Year of Deployment	Complete Years With Data
AM01			2002/2003	
Top	15/01/2002	440	T, S, P	2002
Middle	15/01/2002	580	T, S	2002–2007
Bottom	15/01/2002	743	T, S	2002–2007
AM04			2006/2007	
Top	11/01/2006	550	T, S, P	2006–2010
Middle	11/01/2006	693	T, S, P	2006–2010
Bottom	11/01/2006	814	T, S, P	2006–2010
AM05			2010/2011	
Top	19/12/2009	580	T, S, P	2010–. . .

[a]T = Temperature; S = salinity; P = pressure.

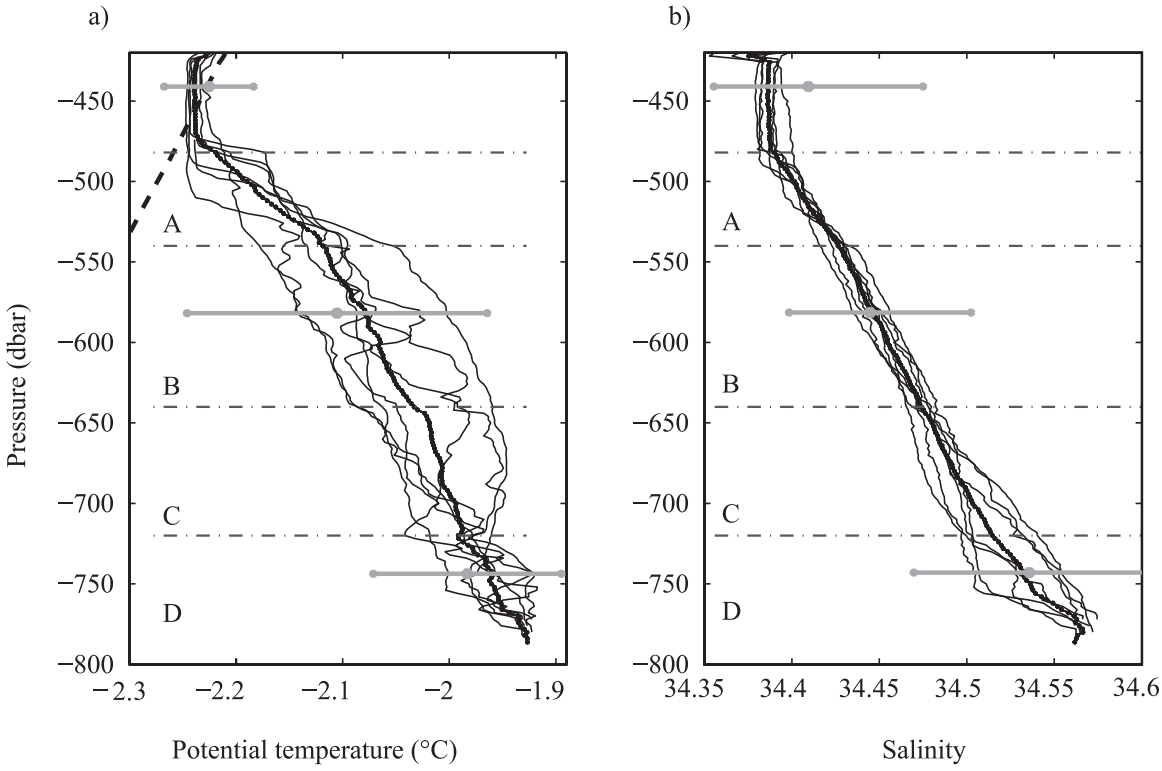

Figure 2. (a) Potential temperature (θ) and (b) salinity (S) CTD profiles at AM01. The thick dotted line depicts the $\overline{\theta}$ and $\overline{S}$ profiles, while the three gray horizontal lines depict the $\overline{\theta} \pm 2^{*}$std ($\overline{\theta}$) (same for $\overline{S}$) of the moored Microcats from 2002. Thin dashed lines delimit sections of the profiles labeled A to D. The potential freezing temperature profile, which is adiabatically referenced to the surface, is shown by the bold dotted line.

column. At AM04 however, the subice shelf bathymetry was deeper than expected and, since the mooring cable was not long enough, the bottom instrument was deployed more than 150 m from the sea floor.

3. Results

3.1. Summer CTD Profiles

[17] Water masses are classified according to their temperature and salinity values, which retain an imprint of the processes that have modified them. The CTD profiles of temperature and salinity provide a snap-shot of the whole water column at AM01. The most prominent feature in the CTD profiles is the presence of a mixed layer occupied by ISW (Figure 2). The mixed layer-thickness is 57 ± 19 m mean thickness, and with a mean and standard deviation in θ and S of -2.23 ± 0.01°C and 34.39 ± 0.002, respectively. The coldest and freshest ISW occupies the mixed layer, and it is super-cooled (below its pressure freezing temperature) in the upper 25 m (Figure 2a, thick dotted line). Although frazil ice can be present under these conditions, no frazil ice was observed suspended in the water column, from video footage taken in the borehole prior to freezing [*Craven et al.*, 2009].

[18] The dependence of the freezing temperature of seawater with depth can be used to determine when the ISW was last modified. The lowest temperature to which a water parcel can be cooled beneath an ice shelf is the in situ freezing point of the deepest ice with which the water parcel has been in contact. Conversely, the minimum depth, D_{min}, of ice shelf base with which a water parcel has interacted, is that for which the in situ freezing point matches the water parcel's potential temperature calculated with reference to D_{min}. Thus, for a water parcel in the mixed layer with an in situ temperature of -2.23°C ($\theta = -2.24$°C), the D_{min} is at 440 dbar (with $S = 34.6$, the saltiest waters seen at AM01). The ice shelf draft at AM01 is 427 dbar, some 13 m shallower. The fact that the top of the mixed layer is already super-cooled at AM01 and that ISW was last modified south of AM01, where the ice shelf base is deeper, suggests that the ISW, in the mixed layer, flows northward past AM01 toward the ice shelf calving front.

[19] HSSW occupies the bottom layer of the water column at AM01 (Figure 3). HSSW forms during the winter months, when brine expelled during sea-ice formation mixes with the ambient water below the surface. Here we define HSSW as a water mass of temperature between the surface freezing point, -1.88°C, and the 50 dbar-freezing temperature (-1.92°C for a surface salinity of 34.3), and salinity higher or equal to 34.5. The ship-based CTD profiles show two well-defined HSSW types at the ice shelf calving front (Figure 4). HSSW at the surface freezing point and with salinity between 34.5 and 34.6 (Figure 4, light blue) is found west of Prydz Bay Mooring 04 (PBM4) (Figure 1, star), in a narrow deep. A slightly cooler HSSW with salinity between 34.5 and 34.56 is found east of

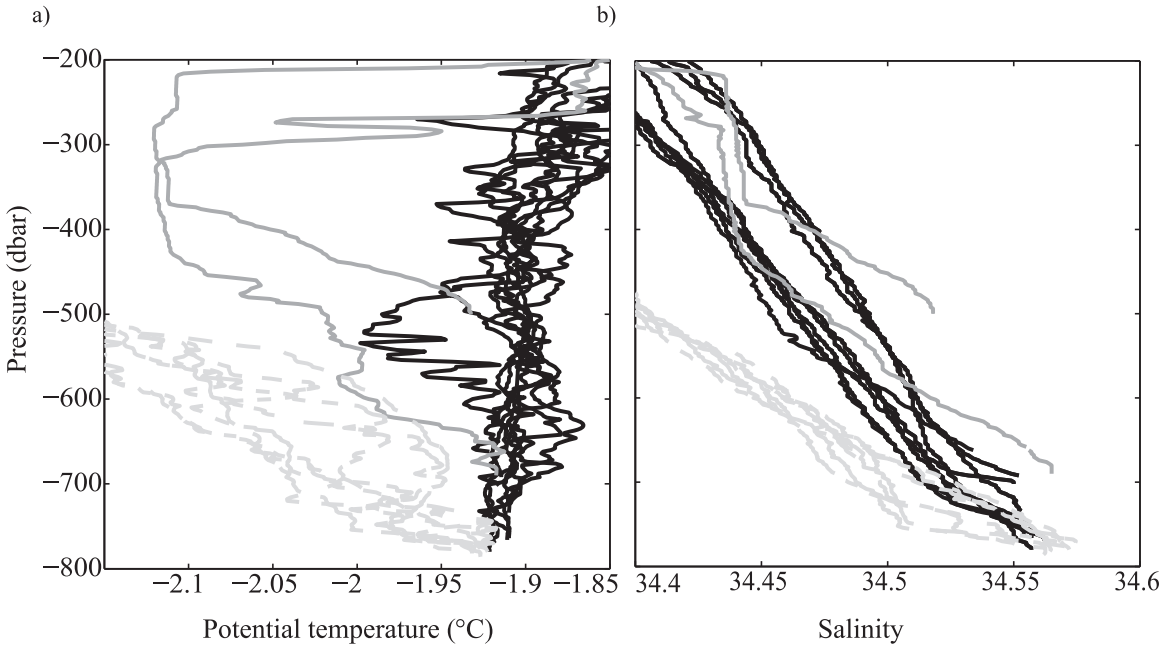

Figure 3. (a) Potential temperature (θ) and (b) salinity in the bottom layer at AM01 (gray dashed lines), and from ship-based hydrographic stations along the eastern AIS calving front, i.e., east of PBM4 (black lines). The two eastern most hydrographic stations to PBM4 are shown in dark gray. No profiles west of PBM4 are shown here.

PBM4 (Figure 4, dark blue). This eastern HSSW has identical θ-S properties to those observed at the bottom layer in AM01 (Figure 3 and 4).

3.2. Seasonal Variability of Temperature and Salinity

[20] ISW and HSSW are the two water masses observed at AM01 throughout the year. We describe the seasonal cycle at AM01 in terms of three periods, which we refer to as the Quiescent Period, the Perturbation Period, and the Transitional Period. These periods are selected to define the main features observed in θ and S during 2002 (Figure 5).

3.2.1. Quiescent Period (January to June)

[21] Two features define this period. The first feature is observed at shallow depths. Within ~20 m of the ice shelf base, the observed ISW stays below its potential freezing temperature (Figure 5, blue and black dashed lines, respectively), with a slowly increasing salinity. In addition, the variability of θ and S is very small. Indeed, the summer CTD profiles show that the shallowest Microcat moored at AM01 was embedded in the mixed layer (Figure 2), and so the low variability in both θ and S at this shallow layer is expected. The second feature is the cooling and freshening trend at intermediate and bottom depths (Figures 5a and 5b, green and red).

3.2.2. Perturbation Period (June to August)

[22] In June, an abrupt increase in temperature and a more gradual salinity increase mark the arrival of HSSW at both the intermediate and bottom depths at AM01 (Figure 5, green and red lines). HSSW occupies a thicker layer than in summer when it was barely 20–50 m (Figure 3, gray). At shallow and intermediate depths, temperature and salinity variability increase considerably, showing highest variability at intermediate depth ($\theta_{std} \pm 0.1$°C, $S_{std} \pm 0.03$). ISW and HSSW intermittently occupy these depths throughout this period (Figure 5, green).

3.2.3. Transitional Period (September to December)

[23] The inflow of HSSW continues until December, although it is mainly restricted to depths greater than 580 dbar. The salinity of the HSSW reaches its peak in October,

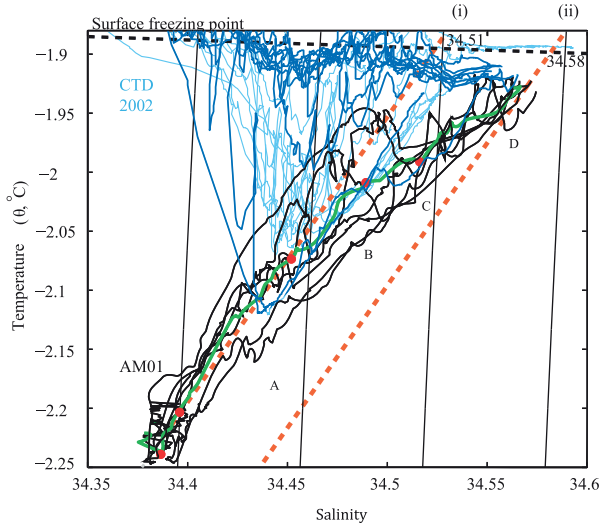

Figure 4. Potential temperature (θ)-Salinity diagram of individual profiles (black solid lines) at AM01. The mean θ-S profile is shown in green. The four regions, A to D shown in Figure 2, are delimited by red dots. Also shown are the θ-S diagram from all the ship-based hydrographic stations along the ice shelf calving front (east of PBM4—dark blue; west of PBM4—light blue). Two Gade lines (equation (1)) are shown as orange dashed lines.

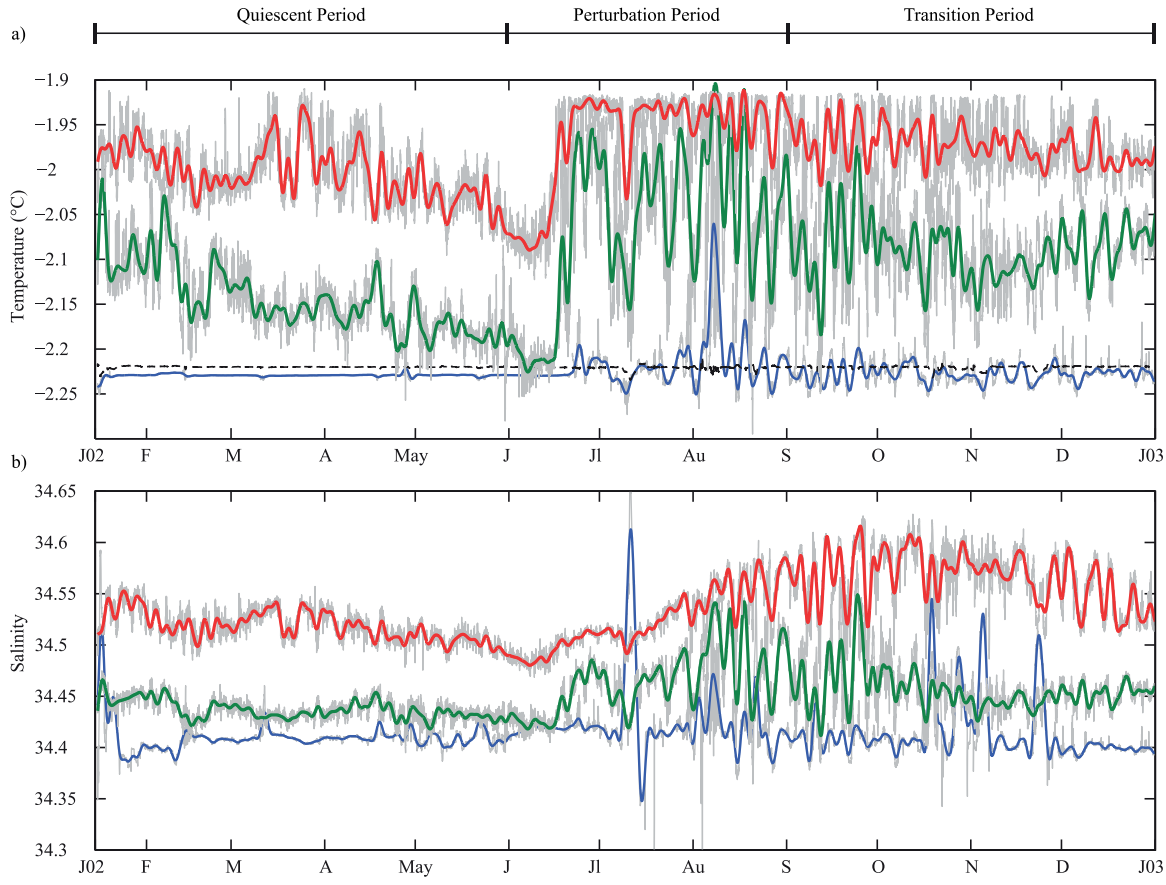

Figure 5. The 2002 record of (a) potential temperature (θ) and (b) salinity at AM01. Each moored Microcat time series is shown in gray with the 40 h Butterworth filtered time series overlaid. Measurement levels are: top (blue, 440 dbar), intermediate (green, 580 dbar) and bottom (red, 743 dbar). The black dotted line is the potential freezing temperature for the observed salinity at the top level.

showing the influence of the on-going sea-ice formation on the overall properties of HSSW as winter progresses (Figure 5, red lines). Also, HSSW is also observed intermittently at the intermediate Microcat (580 dbar) (Figure 5, green). At intermediate depths, the θ-S variability of the ISW is now lower; during October/early November, θ and S decrease, with the θ-S characteristics following a melt-freeze line with a slope of 2.34°C (determined by equation (1), below). Such a slope is indicative of a low vertical temperature gradient in the basal ice ($\sim$ no transfer of heat into the ice), consistent with the site being downstream of an area of marine ice formation. Within 20 m of the ice shelf base, positive salinity excursions become larger and more frequent than during the Perturbation Period, especially during October and November (Figure 5, blue lines). In addition, the isopycnals between AM01 and AM04 flatten and the overall stratification moves toward the "unperturbed" state observed in the Quiescent Period at the beginning of the year.

4. Discussion

4.1. Source Water for the Observed ISW

[24] In θ-S space, the slope of a straight line describes the evolution of the mixing between glacial melt-water and the ambient ocean beneath the ice shelf to form ISW. This line is known as the melt-freeze line or Gade line [*Gade*, 1979] and it is defined by,

$$\frac{d\theta}{dS} = \frac{L}{S_0 c_w} + \frac{(\theta_f - T_i)c_i}{S_0 c_w} + \frac{(\theta_0 - \theta_f)}{S_0} \quad (1)$$

where L is the latent heat of fusion for ice (3.35×10^5 J kg^{-1}); θ_0 and S_0 are the potential temperature and salinity, respectively, of the source water; c_w and c_i are the specific heat capacity of water and ice (4000 and 2010 J kg^{-1}°C^{-1}, respectively); θ_f is the potential freezing temperature at the ice shelf base; and, T_i is the temperature of the basal ice (here we use the temperature of the glacial ice, −15°C, measured from a thermistor cable at AM01). The first term in equation (1) comes from the energy necessary for the change of state (melting/freezing). This term dominates at $\sim$2.4°C. The second term is from the heat necessary to warm the ice to its melting point; and the third term is due to the cooling of the ambient water to its freezing point. The latter is the smallest term ($\sim$2 orders of magnitude smaller than the first).

[25] *Nøst and Foldvik* [1994] showed that, to first order, ISW properties depend on the θ-S of the source water mass that produced it, and are almost independent of entrainment

and melt rates. Thus, further mixing of ISW with its source water has little or no effect on the $\frac{d\theta}{dS}$ described by equation (1). Equation (1) cannot be used to determine the θ-S of the source water from those of the ISW when the mixing of ISWs of different source water salinities occurs or when ISW exits the cavity and is modified by, e.g., atmospheric warming, and then re-enters the cavity. With this in mind, we discuss the possible source water mass of the observed ISW.

[26] HSSW is the source water mass for the ISW observed at AM01. Equation (1) links the ISW and its source water mass, through the melt-freeze line whose slope is given by $\frac{d\theta}{dS}$ [*Gade*, 1979]. Thus, in order to identify the source water mass for the ISW at AM01, two melt-freeze lines are shown: one passing through the coldest and freshest HSSW (θ_0, S_0) (Figure 4, orange dashed line (i)), and the other passing through the HSSW (θ_0, S_0) at the bottom of the water column in AM01 (Figure 4, orange dashed line (ii)). The ISW at AM01 falls approximately between these two melt-freeze lines, pointing to HSSW of salinity spanning from 34.5 to 34.6 as the source water mass. This HSSW is of considerably lower salinity than the HSSW observed, e.g., in the Weddell Sea (salinity up to 34.84) [*Nicholls et al*., 2009]; and in the Adélie Depression (salinity of up to 34.7) [*Williams et al*., 2008]. The melt-freeze line (ii) suggests that the HSSW (of S $\sim$ 34.6) should form an ISW of θ and S falling along line (ii), but no such ISW is seen at AM01, or at any of the other AMISOR boreholes (not shown). Worth noting is the fact that deviations from the melt-freeze line occur when ISW mixes with water masses with different source water salinities. This might be the case for the ISW below the pycnocline, which shows a broad range of θ and S.

[27] HSSW is the densest water mass in Prydz Bay. The circulation path of HSSW is dominated by the local bathymetry, which favors HSSW flow into the AIS cavity through the eastern flank of the ice shelf front toward AM01 (Figure 1). To test this flow, the ship-based CTD profiles taken along the ice shelf calving front (Figure 1, gray dots) are compared with those obtained from AM01, having been both measured in February 2002, within a few days of each other. The eastern HSSW is mixed with ISW and its temperature is just below the surface freezing point. This mixing is likely the result of water moving back and forth across the ice shelf front, albeit with an overall flow into the cavity. The similarity in the HSSW properties between AM01 and the eastern ice shelf front during austral summer shows that HSSW remains in Prydz Bay months after the end of active sea-ice formation, allowing a flow of HSSW into the cavity even in summer.

4.2. Variability of Temperature and Salinity During Summer

[28] The variability in the θ-S profiles at a fixed depth (Figure 2) can be explained by vertical displacements of the water column (e.g., by internal waves), and/or horizontal displacements (e.g., advection of new water masses by tides or currents). Here we follow the method used by [*Pingree*, 1972] and [*Nicholls and Jenkins*, 1993] to diagnose potential causes of the observed variability in the temperature and salinity. First, the ensemble θ-S mean of the 7 casts was calculated and removed from each temperature and salinity profile. For a given depth, the scatter in the θ-S anomaly pairs is assumed to arise from vertical displacements if the scatter lies parallel to the mean θ-S for that depth range, or from horizontal displacements (intrusions) if the scatter lies parallel to the local isopycnal.

[29] Four layers can be distinguished in the mean θ-S diagram (Figure 2), and are analyzed independently. Each layer shows an inherent high variability. We expect that the variability in layer A (Figure 6a) is caused by vertical displacements (e.g., internal waves) as this would explain the heaving (up to 40 m in a single event) of the mixed layer base easily seen in the θ profiles (Figure 2a). Notably, internal wave activity causes much of the variability observed beneath the Filchner-Ronne Ice Shelf [e.g., *Nicholls and Jenkins*, 1993]. However, the scatter along the local θ-S (Figure 6a, dashed line) suggests horizontal displacements may be at play (e.g., tides).

[30] Variability in layer B mainly shows anomalies running parallel to the slope of the local isopycnal, indicating intrusions (isopycnic motion of a different water mass) (Figure 6b). Variability in layer C also appears to be mainly driven by vertical displacements, however the large scatter seen within these layers suggests that horizontal displacements may also be important. The ISW temperature in layers B and C is relatively warm (close to the surface freezing temperature). Mixing along isopycnals between "warm" continental shelf water and ISW would occur very rapidly, resulting in an ISW "anomalously" warm compared with the ISW prior to mixing, as we see in Figure 2a, and further supported by the evidence of advection processes in Figure 6b. The wide range of temperatures seen within the layers (Figure 2a) suggests that at least part of the flow at these layers is toward a deeper part of the cavity.

[31] A combination of processes also explains the variability in layer D. However, the scatter in θ-S anomalies is smaller here than in the other layers. A very thin bottom layer is observed in some profiles but absent in others. The fact that the CTD profiles never reached the sea-floor (mean distance from the bottom of $\sim$15 dbar) is a possible explanation for this apparent absence. The depth of the top of the bottom layer varies from one profile to another during the few days of CTD profiling. The variability seen in layer D (Figure 6b) is mostly a result of heaving of the isopycnals. Heaving, together with the downslope HSSW flow, can cause small vertical displacements at upper (less dense) layers potentially explaining the broader S ranges in layers C and D (Figures 6c and 6d).

4.3. Circulation Within the Cavity Inferred From Subice Shelf Moorings

[32] The annual changes in the temperature and salinity field along AM01 and AM04 are used to infer the most likely circulation pattern beneath the AIS. To aid the discussion, a schematic of the stratification, using the θ and S data from both AM01 and AM04, is shown in Figures 7a–7c. Although these instrumented moorings were deployed through the ice shelf in different years, the properties at AM04 show small inter-annual variability (not shown), and we believe the data from both sites to be comparable. Potential density values for the month representative of each of the three periods described in section 3.2

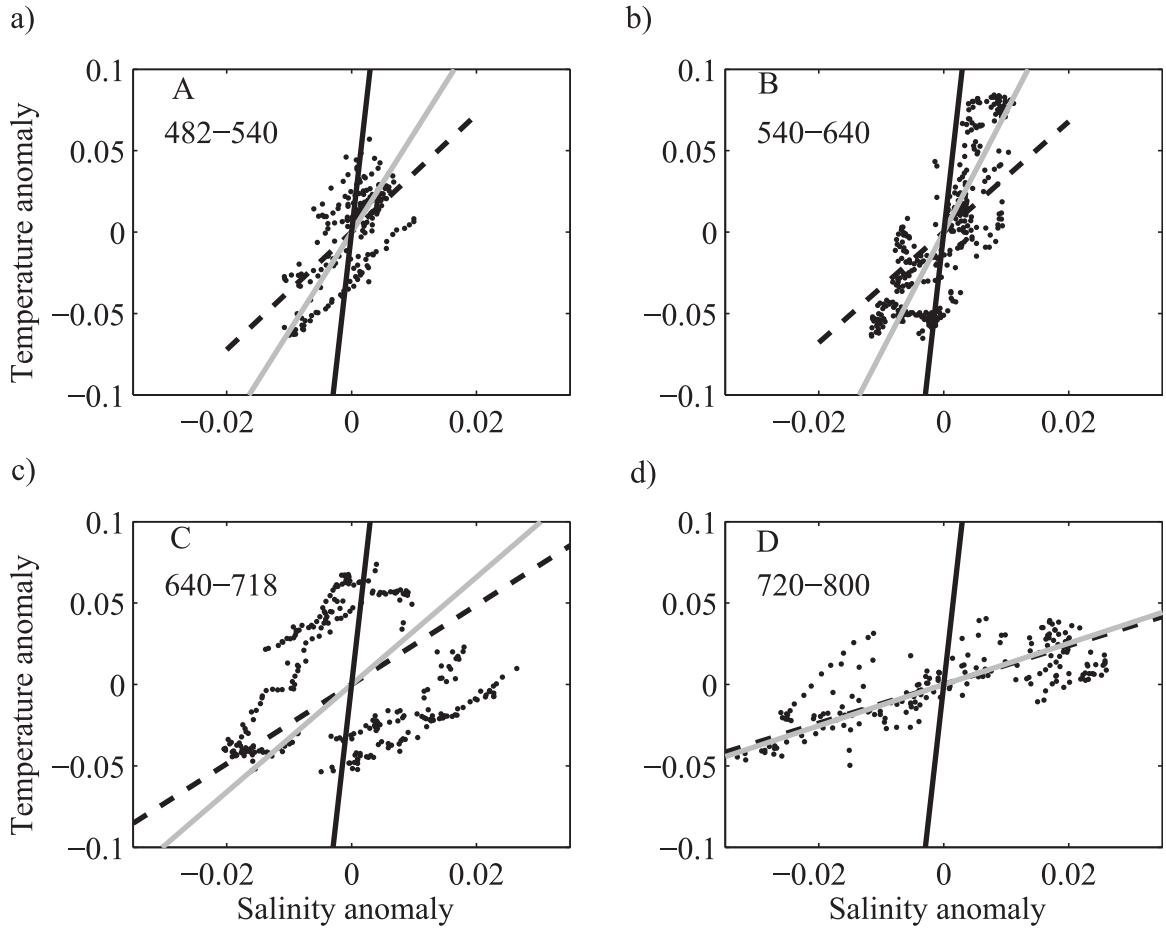

Figure 6. Scatter plots for potential temperature-salinity anomaly pairs using 2-dbar bins. Each subplot refers to one of the 4 sections (A–D) shown in Figure 2, whose pressure interval (dbar) is shown in the top left corner. The black solid line is the gradient of the local isopycnal, the dashed line is the θ-S gradient for the section, and the gray line is the best fit through the anomaly pairs. If the best fit coincides with the local θ-S characteristic, the variability probably results from vertical advection (e.g., internal waves). A best θ-S fit parallel to the local isopycnal suggests horizontal intrusions.

(Perturbation, Transitional, and Quiescent) were used to present a simplified view of the density field.

[33] The AIS cavity fills with ISW as the inflow of HSSW decreases during the Quiescent Period (January to June). Following the slowdown of HSSW inflow into the cavity, a gradual decrease in temperature and salinity occurs at both intermediate and bottom depths (Figure 5), which is likely the result of ISW filling up the cavity. In addition, a layer of super-cooled water lies just beneath the ice shelf base (Figures 2 and 5a, blue). At this temperature ($\theta < \theta_f$), the formation of frazil ice is possible. Indeed, several super-cooling events precede salinity increases throughout this period at AM01 (Figure 5, blue lines). The change in temperature and salinity follows the Gade line, suggesting local formation of frazil ice.

[34] A layer of super-cooled water protects the ice shelf base from the advection of heat from greater depths. A layer of super-cooled ISW is observed within 20 m of the ice shelf base in every mooring deployed where the marine ice layer is present, that is AM01, AM04, and AM05. This layer is clearly seen in AM01 (Figures 2a and 5a, blue). Moreover, the cooling/freshening of the water column below the top Microcat (by the filling of the cavity with ISW) prevents warm waters from reaching the marine ice layer during this period at AM01, and throughout the year at AM04 and AM05 (not shown). In June, before the arrival of HSSW at AM01, the temperature and salinity at shallow and intermediate depths match, suggesting a deepening of the (summer) mixed layer, making it at least 160 m thick.

[35] The arrival of HSSW at AM01 is followed by changes in the overall variability in θ-S, especially at intermediate depths. From June to October high variability in the θ-S results from ISW and HSSW intermittently occupying the intermediate layers (Figure 7e, green squares). This variability in θ-S suggests that the inflow of HSSW is an eddy-like flow, as the HSSW inflow becomes baroclinically unstable at the ice shelf calving front. *Nicholls* [1996] gave evidence of such instabilities under the Filchner-Ronne Ice Shelf. Recently, *Årthun et al.* [2013], using a high-resolution model, showed that eddy-driven HSSW inflows result from frontal instabilities, with periods of 5–6 days. Figure 8 shows enhanced energy linked to periods between 2 and 8 days during the austral winter, when the arrival of HSSW is observed in AM01. This confirms that eddy-

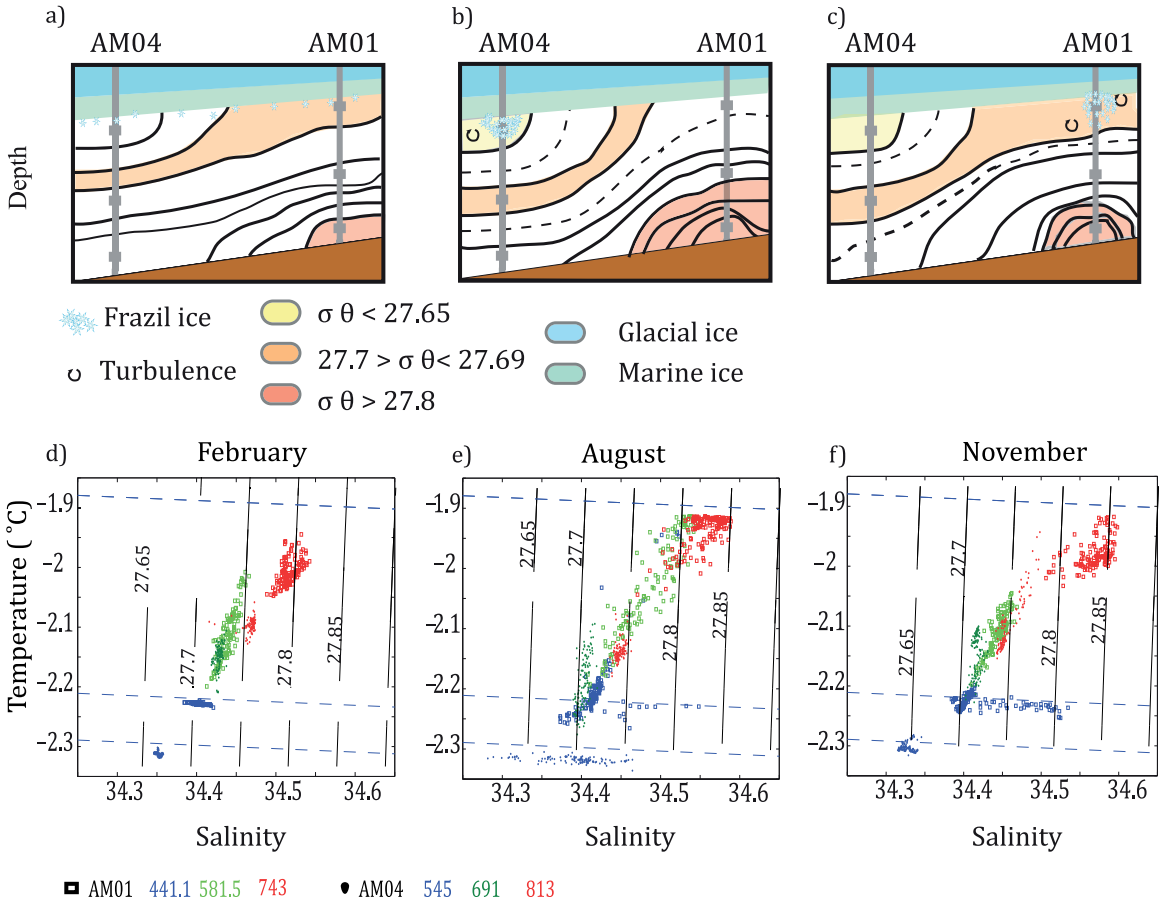

Figure 7. Seasonal change in stratification between AM01 and AM04. Top: Density contours during (a) February, (b) August, and (c) November. Black lines depict isopycnal intervals of 0.02 kg m^{-3}, while dashed lines depict 0.01 kg m^{-3} intervals. Three density ranges are highlighted to aid interpretation (yellow, orange and red). Bottom: θ-S diagrams (from 6 hourly measurements) at AM01 and AM04 during (d) February, (e) August and (f) November (color code is the same as Figure 5). The blue dotted lines are the potential freezing point at 0, 440, and 545 dbar (from top to bottom, respectively).

driven flow as a result of baroclinic instabilities at the ice shelf calving front is responsible for the HSSW inflow and the observed variability at intermediate and bottom layers during the winter months (Figure 5, green and red lines). Changes in stratification also result from the arrival of HSSW at AM01.

[36] A simplified view of the seasonal evolution of the stratification between AM01 and AM04 reveals an interesting feature: an apparent steepening of the isopycnals toward the ice shelf base is observed following the arrival of HSSW. This steepening potentially provides a path for ISW to reach the ice shelf base more quickly than during the previous period, impacting the formation and accretion of frazil ice. Indeed, the θ-S characteristics at intermediate depths at AM04 (Figure 7e, dark green dots) are identical to those seen in the shallowest layer at AM01 (Figure 7e, dark blue squares). Following the sketch shown in Figure 7b and at intermediate depths, the AM04 ISW could reach shallower depths, and therefore a new in situ freezing temperature, causing the formation of frazil ice.

[37] Our multiyear data record (not shown) indicates that inflow of HSSW into the AIS cavity has considerable interannual variability. Table 3 shows the month of arrival of HSSW at AM01, defined as an abrupt increase in temperature toward the surface freezing temperature. This variability will most likely have an impact on the steepening of the isopycnals described here, and potentially, on variability in the formation of marine ice.

4.4. Variability in the Accretion of Frazil Ice to the Marine Ice Layer

[38] The Amery Ice Shelf marine ice accounts for about 9% of the ice shelf volume [*Fricker et al.*, 2001]. The marine ice layer is up to 200 m thick, such as at borehole sites AM01 and AM04 [*Fricker et al.*, 2001]. The accretion of marine ice at the base of the Amery Ice Shelf commences ~350 km downstream of the southern limit of the grounding zone, at a point where the ice thickness has decreased to 700 m from an initial value of 2500 m, as a result of basal melting and strain thinning [*Craven et al.*, 2009].

[39] Processes driving variability in the formation rate of marine ice as well as the sensitivity to ocean variability are largely unknown. The difficulty in accessing and observing the formation of marine ice has been the major obstacle to improving our understanding of these processes. The

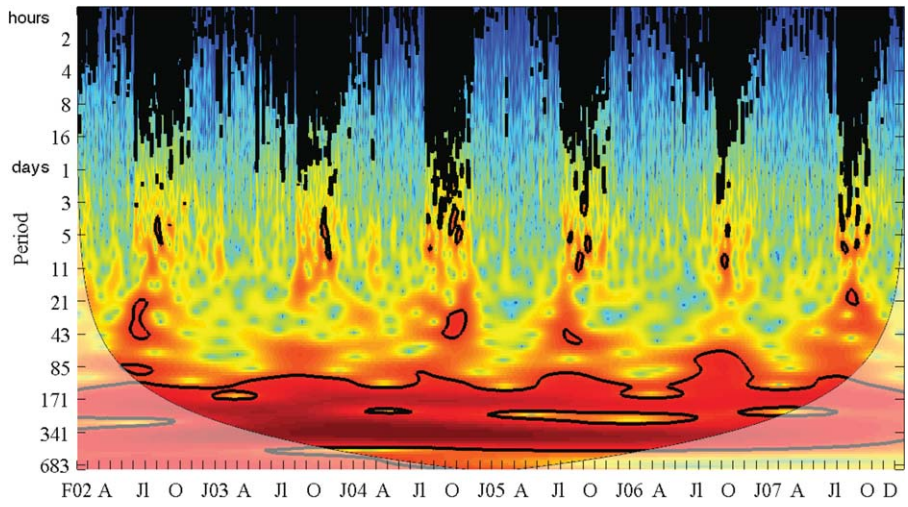

Figure 8. Wavelet analysis of the temperature time series at intermediate depth in AM01. All areas enclosed by the solid black lines are statistically significant at the 95% level.

principal condition for frazil ice to be present is that the ISW temperature is at or below (super-cooled) its pressure freezing temperature. This condition is met for most of the year in at least the top 20 m of the water column at both AM01 and AM04 (section 4.3, Figures 6a, blue, and 8). Also, accretion of the majority of the suspended frazil ice is thought to occur in spatially discrete bursts [*Bombosch and Jenkins*, 1995]. Other variables such as the ISW plume velocity, frazil ice size, and ice shelf base draft provide additional controls over the formation of frazil ice and its deposition at the ice shelf base [e.g., *Bombosch and Jenkins*, 1995; *Smedsrud and Jenkins*, 2004].

[40] The seasonal changes in the potential temperature and salinity suggest that the formation of marine ice is also seasonal. The stratification adjusts itself by the steepening of the less dense isopycnals toward the ice shelf base from AM01 to AM04 (Figures 7b and 7f). This new stratification provides a path for ISW to "upwell" and reach the pressure freezing temperature, and thus for frazil ice to form independently of the shape of the ice shelf base (provided there is a seed to start nucleation). This process highlights the fact that for frazil ice to form, the ISW does not need to be in contact with the ice shelf base and that it is likely subject to seasonal variability. Note that the potential temperature of the upwelling ISW plume must be equal to or lower than the new pressure freezing temperature for it to become super-cooled, as is the case here (Figure 7e). Interestingly, salinity excursions ($\Delta S > +0.05$) are also measured within $\sim$20 m of the ice shelf base concurrently with, and shortly after, the steepening of the isopycnals at AM01 (Figures 6 and 7d–7f, blue). In addition, similar positive salinity excursions are observed at AM04 and AM05. There are several potential explanations for the salinity excursions, and their seasonal variability, and these are discussed next.

[41] First, a source water of salinity $\sim$34.7 could form ISW of such high salinity. However, we have no evidence of any such water mass either beneath the ice shelf or in Prydz Bay.

[42] Second, brine rejection from the marine ice layer during consolidation might be responsible: although consolidated marine ice has a lower salinity than sea ice [*Tison et al.*, 1993], newly deposited ice would be expected to have significantly higher salinity inclusions. Deposition of new ice to the marine ice layer could squeeze the mushy layer and help expel partially trapped brine [*Eicken et al.*, 1994]. However, given that the Microcat is positioned $\sim$20 m below the ice shelf, it would appear unlikely that streamers of expelled brine would reach the instrument without being dispersed.

[43] A third possibility is brine rejection during frazil ice formation in the water column. The salinity variability included sporadic events during which the excursions in salinity were as high as +0.24 (Figure 5b, blue line). The duration of these events varied from 1 day to several days (e.g., August and October events, Figure 5b, blue line) during which the temperatures also rose from below, to just at, the freezing temperature. Such a salinity rise would require up to 0.14 m equivalent of frazil ice formation (for a 1 m^2 by 20 m thick water layer, the distance between the shallow Microcat and the ice shelf base). The changes in θ/S do not, however, lie on the melt-freeze line. Indeed, the fact that frazil ice forms at one location does not imply that it will accrete at the same spot. If conditions are favorable, an ISW plume can carry frazil ice crystals for some distance before they settle out of the plume and accrete at the ice shelf base.

[44] Finally, suspended frazil ice crystals could flow through the conductivity cell and compromise the conductivity measurements. Anomalously low salinity measurements are expected to occur when ice crystals flow through the conductivity cell. Anomalously high salinity values, though, are harder to explain. Ice crystals could also scour away the cell, resulting in higher than normal salinity

Table 3. Month of the Arrival of HSSW at AM01 From 2002 to 2007

	2002	2003	2004	2005	2006	2007
HSSW Arrival	Jun	Aug	Jul	Jul	Aug	Jul

measurements. However, the salinity seems to return to normal values. In addition, similar anomalous salinities (ΔS) have been observed at the other borehole sites with a marine ice layer, namely AM04 and AM05 (Figures 9b and 9c, respectively). These ΔS events appear as outliers in Figure 9 (gray crosses). Both low and high ΔS events are mainly seen during the austral winter, especially in AM04 and AM05; while, in AM01, high ΔS events are seen mainly in late winter (Figure 9). The pressure showed high variability concurrent with the low and high ΔS events, however, no significant pressure changes were observed at any of the time series used here. Conversely, none of the three ice shelf cavity mooring sites on the eastern side of the AIS where there is no marine ice layer present (not shown) show such ΔS events.

[45] Two processes explain the observed seasonal variability in the marine ice layer formation. (i) A peak in HSSW-driven basal melt is likely to occur during the austral summer. Together with a lower inflow of HSSW, the overall cooling and freshening in the water column at all six sites from approximately January to June provide the ideal conditions for frazil ice formation, advection and, in turn deposition. In addition, convective mixing driven by brine rejection during frazil ice formation explains the mixed layer deepening ∼160 m by the end of June, observed at AM01. This deepening is likely to be a gradual process as the ISW plume moves from the inner part of the cavity to the open ocean. This process is likely to dominate the seasonal signature seen at AM04 and AM05. (ii) Temperature and salinity at AM01 show a strong seasonal variability due to its close location to the open ocean. We have shown that the arrival of HSSW at AM01 drives a stratification change between AM01 and AM04, which in turn allows ISW to follow isopycnals that steepen toward the ice shelf base. This process allows frazil ice to form during the austral winter, and contribute to the ΔS observed at AM01. However, as the seasonal cycle of the temperature and salinity is larger in AM01 than at AM04 and AM05 and the influence of external forcing is also large, we cannot discard other processes.

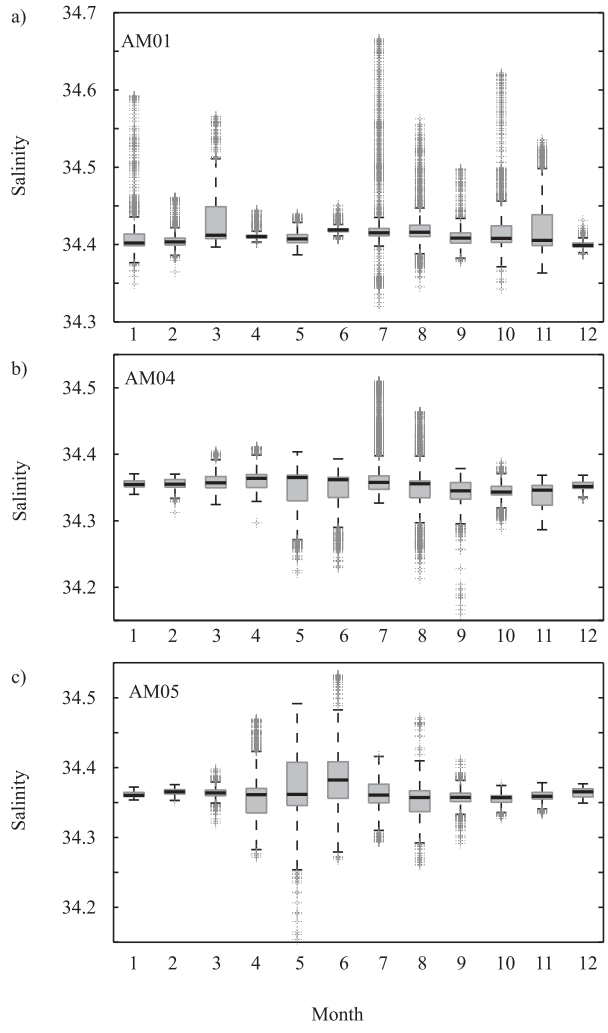

Figure 9. Composite seasonal cycle of salinity within ∼20 m of the shelf base at the three sites (AM01, AM04, and AM05) with a marine ice layer present. The black bars show the monthly median S. The height of the box depicts the 25% and 75% percentile. Outliers are shown as crosses.

4.5. Interaction Between Continental Shelf Waters and the AIS Cavity

[46] The seasonal cycle of sea ice exerts a powerful influence over the ocean around Antarctica and it is a key process in the global ocean circulation. The waters in the cavity of the AIS respond quickly to the formation of sea ice, and we now explore the response of the spatial pattern to sea ice variability using the data collected at AM01 and PBM4. The PBM04 data are not representative of all Prydz Bay, but do give valuable information about the variability in the water column at the front of the AIS. We describe the annual sea-ice cycle as four stages (following *Williams et al*., [2008]): conditioning (C), formation (F), peak (P), and destruction (D). Each of these stages is clearly observed in the temperature and salinity time series from PBM4 (Figure 10, top labels). In July, the increase in the water column salinity at PBM4 shows that sea-ice formation (F) has already started (Figure 10b, black solid dotted line). Further ocean surface cooling allows sea ice to form until October when the peak in sea-ice formation (P), characterized by a salinity maximum, is reached. θ and S at intermediate and bottom depths at AM01 respond almost synchronously to this forcing (within interannual variability), highlighting the rapid transmission of open ocean variability to the AIS cavity (Figures 6 and 10b). Such rapid response to the sea-ice cycle has been previously reported beneath other ice shelves such as the Filchner-Ronne Ice Shelf [e.g., *Nicholls and Makinson*, 1998].

[47] The variability of the ocean in Prydz Bay is in turn strongly linked to the subcavity ocean variability. ISW exits the AIS cavity in two main areas close to the western edge of the AIS calving front (not shown) and at the middle of the ice shelf front at PBM4. From January to June, ISW at PBM4 cooled and freshened toward the ISW properties at AM01 and their respective θ-S properties are linked by the melt-freeze line, suggesting that at least part of the ISW seen at AM01 exits in the vicinity of PBM4. Figure 10 shows the almost synchronous (within interannual variability) cooling and freshening from the deepest moored instrument at both sites. Conversely, in the second half of the year, the arrival of HSSW at AM01 dominates the

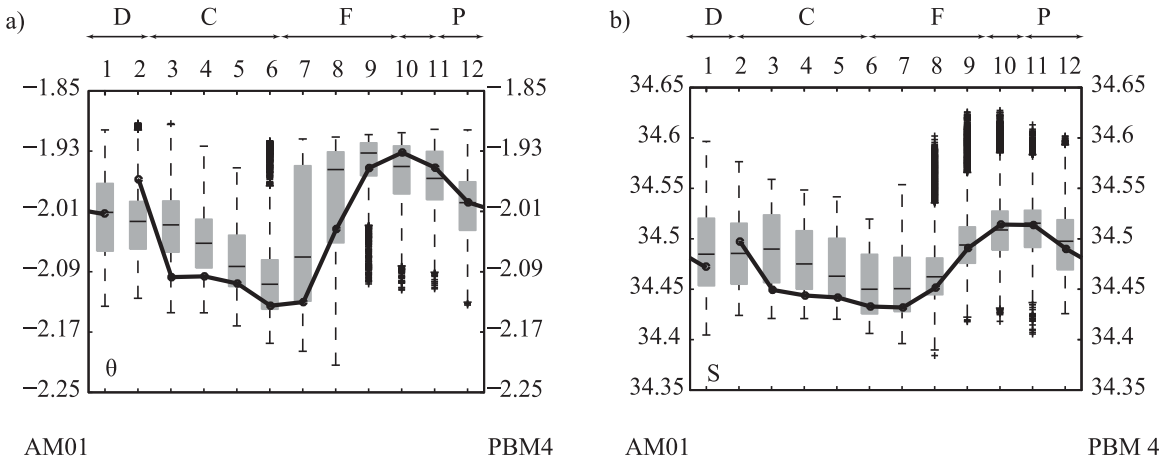

Figure 10. Composite monthly (a) potential temperature (θ) and (b) Salinity (S) at the deepest Microcat (743 dbar) at AM01 (left-hand scales). The black bars show the monthly median θ and S. The height of the box depicts the 25% and 75% percentile per month. The thick black dotted line is the monthly $\overline{\theta}$ and $\overline{S}$ at 525 m (within ∼10 m of the bottom) at PBM4 (right-hand scales). Correlation of monthly θ and S between AM01 and PBM4 is significant at the 99% confidence level. The sea-ice annual cycle is divided into 4 stages: D, destruction; C: conditioning; F: formation; P: peak.

variability there. This shift in variability implies a change in the circulation from being mainly outflowing ISW from January to June to both, (i) outflow of ISW at depths no deeper than ∼581 dbar (the depth of the middle Microcat) and (ii) inflow of HSSW below this depth.

5. Conclusions

[48] Temperature and salinity observations from beneath the Amery Ice Shelf provide new information on ice shelf-ocean interaction and its seasonal variability. The observations were obtained from three instrumented moorings deployed through hot water-drilled boreholes at sites AM01, AM04, and AM05, where a thick layer of marine ice underlies the meteoric ice. Additional data along the AIS calving front complement our analyses. The main conclusions are:

[49] 1. HSSW is the source water of the observed ISW at AM01. HSSW is observed beneath the AIS all year round. In the austral summer, HSSW forms a 20 to 50 m thick bottom boundary layer, and enters the AIS across the eastern edge of the calving front. In the austral winter, the HSSW layer increases in thickness, arriving at AM01 abruptly as an eddy-rich flow. These eddies are caused by baroclinic instabilities as the newly formed HSSW layer enters the cavity, influencing at least the bottom ∼200 m of the water column.

[50] 2. The formation of the marine ice layer beneath the Amery Ice Shelf is subject to seasonal variability. This seasonal variability is driven by the response of the ocean beneath the Amery Ice Shelf to the seasonal changes in the inflow of HSSW.

[51] 3. Super-cooled ISW forms a boundary layer just beneath the marine ice layer at AM01 all year round, insulating the permeable marine ice layer from the warmer waters beneath. This boundary layer is embedded in a mixed layer ∼50 m thick (in February 2002). The thickness of this mixed layer increased from January to June to a maximum of ∼160 m in June (2002). Two processes explain the thickening of the mixed layer. First, as the inflow of HSSW decreases, ISW refills the cavity, cooling and freshening the water column. Second, the formation of frazil ice occurs during this period, causing convective cells as a result of brine rejection and entraining saltier water from below. The upper part of the boundary layer filled with super-cooled water is also observed against the ice shelf at borehole sites AM04 and AM05, where a marine ice layer is also present.

[52] 4. Changes in the stratification of the water column due to HSSW inflow may impact the formation of frazil ice and its deposition. Following the arrival of the newly formed HSSW at AM01 in the austral winter, the stratification of the water column between AM01 and AM04 changes. Less dense isopycnals outcrop toward the ice shelf base allowing ISW to upwell and reach a new pressure freezing temperature. We argue that the upwelling ISW results in frazil ice forming at likely higher rates than previously expected. The shape of the ice shelf base is usually regarded as an important factor in frazil ice formation and deposition. However, this new mechanism depends only on the inflow of HSSW beneath the Amery Ice Shelf, which at AM01 shows high interannual variability.

[53] To develop a complete picture of the Amery Ice Shelf-ocean interaction, it is essential that both ocean variability in Prydz Bay and beneath the Amery Ice Shelf are jointly considered. The timing and duration of outflow of the ISW (∼7 months at PBM4) will play a critical role in conditioning the water column prior to the start of sea-ice formation, and thus is likely to affect total sea-ice formation in Prydz Bay. Improved understanding of this coupling is critical if we are to understand the high interannual variability seen in the inflow of HSSW (Table 3), its effect on the net basal melt of the AIS, and also its overall role in the variability of the marine ice thickness. This work highlights

the vulnerability of the marine ice layer to short-time scale changes in the ocean variability outside the AIS cavity.

Appendix A: Data Processing and Quality

[54] The information provided here has been taken from the following internal report: Amery Ice Shelf experiment (AMISOR)—marine science cruises au0106 and au0207—oceanographic field measurements and analysis, Research Report 30, Antarctic Cooperative Research Centre, Hobart, Australia.

A1. FSI microCTD Processing and Calibration

[55] Preseason laboratory calibrations of the FSI microCTD temperature, pressure and conductivity sensors were done at the Commonwealth Scientific and Industrial Research Organization (CSIRO). In the field, data were output from the FSI microCTD in engineering units, with CSIRO calibration coefficients applied for temperature, pressure and conductivity. Further corrections for pressure and conductivity were obtained from in situ measurements, as detailed in the next section.

[56] Three casts were obtained during the au0207 oceanographic cruise onboard the R/V *Aurora Australis*. For these three casts the FSI microCTD, in internally recording battery-powered mode, was attached to the ship's main rosette system, and three routine 12 bottle casts were taken with General Oceanics (GO) CTD serial 2568. FSI and GO CTD data were then compared, and FSI conductivity data were calibrated against the bottle samples obtained. The following processing steps were followed for the three au0207 casts to obtain calibration corrections for the FSI pressure and conductivity:

[57] 1. Surface pressure offset was found by averaging the 20 pressure points previous to the CTD entering the water. This offset was then removed from FSI pressure data.

[58] 2. Upcast burst data were formed by retaining the 30 s of data previous to each bottle firing, then averaging these 30 s bursts. Burst averages were then merged with GO upcast burst averages, and salinity bottle data.

[59] 3. Separate pressure monotonic files were formed for downcast and upcast data.

[60] 4. Comparison of FSI and GO pressure data revealed a small calibration difference, of the order 4 dbar over 2000 dbar. Assuming GO pressure as the more accurate, a correction was found for FSI pressure as follows. The upcast pressure burst averages for the FSI CTD were linearly fitted to the GO pressure burst averages. The following linear correction was then applied to all FSI pressure data:

$$p_{cal} = 1.0020\ p_{raw} + 0.2506 \quad \text{(A1.1)}$$

[61] 5. where p_{cal} and p_{raw} are, respectively, the corrected and uncorrected FSI pressure. Note that when obtaining the best-fit, equal weight was given to both a fit through 0 pressure at the surface, and to the rest of the pressure data. However, application of this pressure correction still causes a small error of ~0.3 dbar to pressures near the surface.

[62] 6. FSI conductivity was calibrated using the salinity bottle data. The three stations were grouped together to provide a single calibration fit (i.e., no station dependent term). The linear correction obtained was:

$$c_{cal} = 0.99662\ c_{raw} + 0.080084 \quad \text{(A1.2)}$$

[63] 7. where c_{cal} and c_{raw} are, respectively, the corrected and uncorrected FSI conductivity; this correction was applied to all FSI conductivity data.

[64] 8. 2 dbar averages were formed for temperature, corrected pressure and corrected conductivity, from the pressure monotonic downcast and upcast files. Note that a minimum attendance of two data points was required to form each 2 dbar bin. A salinity value for each 2 dbar bin was then calculated from these averages.

[65] Good salinity samples were obtained from the Niskin bottles deployed through the borehole site AM01, allowing an additional correction to be applied to FSI conductivity data. Salinity ranges below the ice shelf were small enough (~0.2 PSS78) that a simple offset correction was adequate. Comparing CTD and bottle salinities, the following offset correction was obtained:

$$c_{newcal} = c_{cal} + 0.0205 \quad \text{(A1.3)}$$

where c_{cal} is the conductivity from equation (A1.2), and c_{newcal} is the final corrected conductivity value (equivalent to a salinity correction of ~0.028 PSS78). This final correction was applied to all borehole CTD conductivity data.

[66] The temperature calibration difference between the two instruments appears to be ~0.003°C for the downcast, and ~0.005°C for the upcast, with significantly greater differences at low temperatures around the temperature minimum. Closer inspection of the vertical temperature profiles for the two CTDs reveals the large temperature difference around the temperature minimum as being due to pressure calibration differences causing vertical offset of the two profiles. And the larger temperature difference apparent on the upcast is again due to pressure calibration differences—in this case there is hysteresis of the pressure sensor for one of the two CTDs, causing increased vertical offset of the upcast temperature profiles for the two instruments. So temperature values for the two CTDs agree to within 0.003°C.

[67] FSI and GO CTD salinities compare reasonably well, to within ~0.003 (PSS78). As above for temperature, the pressure calibration differences exaggerate the salinity difference around steep vertical gradients.

A2. Subice Shelf Moorings in Borehole Site AM01

[68] No discontinuities were present in the first download of Microcat data from AM01, that is, from 2002 to 2003.

[69] Manufacturer supplied calibrations (May/June 2001 for AM01 instruments) were applied internally by the Microcats, and calibrated data were output. The raw files were manually edited to remove data where the Microcats were being deployed.

[70] A brief comparison was made between borehole Microcat and CTD temperature and salinity data. Although no simultaneous Microcat and CTD measurements exist, the time difference was only of the order of several days, and a valid comparison can still be made in TS space.

Fairly good agreement was found between the CTD and Microcat data for borehole AM01 in the 2002/2003 season.

[71] For AM01, the pressure sensors were faulty for the intermediate and bottom Microcats, although a small amount of reliable pressure data were recorded for the first few days after initial deployment. Consequently, pressure/depth values used for AM01 Microcat data are determined from the first few pressure sensor values after deployment. Salinity and conductivity values for the AM01 Microcat data are recalculated using these constant pressure values, except for the shallowest Microcat where the measured pressure data were used.

A3. Salinity Error Due to Pressure

[72] For AM01, constant pressure values (derived from the first few readings after deployment) were used for the recalculation of conductivity and salinity, as discussed previously. As pressure fluctuations for AM01 are unknown, a small salinity error is therefore expected. For AM01, at the local conditions of conductivity $\sim$27 mS/cm and temperature $\sim -2^{\circ}$C, omission of pressure fluctuations of up to 3 dbar from salinity calculations would result in a maximum salinity error of $\sim$0.002 (PSS78). For those pressure changes of up to $\sim$17 dbar, salinity calculations would result in a maximum salinity error of $\sim$0.01 (PSS78) (at intermediate and bottom Microcats).

[73] Additional salinity errors for AM01 might arise from unknown mean vertical changes in mooring position over the years. The salinity error resulting from a 1 to 2 dbar pressure change is considered negligible here.

[74] **Acknowledgments.** [74] We thank two anonymous reviewers and the editor for their thorough and helpful comments on an earlier version of the manuscript. This work was supported by the Australian Government's Cooperative Research Centers Program through the Antarctic Climate and Ecosystems Cooperative Research Centre (ACE CRC). We acknowledge logistic support from the Australian Antarctic Division (AAD) and valuable input from the many people who have contributed to the Amery Ice Shelf Ocean Research (AMISOR) ASAC1164 field program.

References

Allison, I. (1979), The mass budget of the Lambert Glacier drainage basin, Antarctica, *J. Glaciol.*, *22*(87), 223–235.

Årthun, M., P. Holland, K. Nicholls, and D. Feltham (2013), Eddy-driven exchange between the open ocean and a sub-ice shelf cavity, *J. Phys. Oceanogr.*, *26*, 2372–2387, doi:10.1175/JPO-D-13–0137.1.

Bombosch, A., and A. Jenkins (1995), Modeling the formation and deposition of frazil ice beneath Filchner-Ronne Ice Shelf, *J. Geophys. Res.*, *100*(C4), 6983–6992.

Budd, W. (1966), The dynamics of the Amery Ice Shelf, *J. Glaciol.*, *6*(45), 335–358.

Budd, W., M. Corry, and T. Jacka (1982), Results from the Amery Ice Shelf Project, *Ann. Glaciol.*, *3*, 36–41.

Clough, J. W., and B. L. Hansen (1979), The Ross Ice Shelf Project, *Science*, *203*(4379), 433–434, doi:10.1126/science.203.4379.433.

Craven, M., I. Allison, R. Brand, A. Elcheikh, J. Hunter, M. Hemer, and S. Donoghue (2004), Initial borehole results from the Amery Ice Shelf hotwater drilling Project, *Ann. Glaciol.*, *39*, 531–539, doi:10.3189/172756404781814311.

Craven, M., I. Allison, H. A. Fricker, and R. Warner (2009), Properties of a marine ice layer under the Amery Ice Shelf, East Antarctica, *J. Glaciol.*, *55*, 717–728, doi:10.3189/002214309789470941.

Eicken, H, H. Oerter, H. Miller, W. Graf, and J. Kipsfstuhl (1994), Textural characteristics and impurity content of meteoric and marine ice in the Ronne Ice Shelf, Antarctica, *J. Glaciol.*, *40*(135), 386–398.

Foldvik, A., and T. Kvinge (1974), Conditional instability of sea water at the freezing point, *Deep Sea Res.*, *21*, 169–174.

Foster, T. D. (1983), The temperature and salinity fine structure of the ocean under the Ross Ice Shelf, *J. Geophys. Res.*, *88*(C4), 2,556–2,564.

Fricker, H. A., S. Popov, I. Allison, and N. Young (2001), Distribution of marine ice beneath the Amery Ice Shelf, *Geophys. Res. Lett.*, *28*, 2241–2244, doi:10.3189/172756402781817581.

Fricker, H. A., et al. (2002), Redefinition of the Amery Ice Shelf, east Antarctica, grounding zone, *J. Geophys. Res.*, *107*(B5), 2092, doi:10.1029/2001JB000383.

Gade, H. G. (1979), Melting of ice in sea water: A primitive model with application to the Antarctic ice shelf and icebergs, *J. Phys. Oceanogr.*, *9*, 189–198, doi:10.1175/1520-0485(1979).

Galton-Fenzi, B., C. Maraldi, R. Coleman, and J. Hunter (2008), The cavity under the Amery Ice Shelf, east Antarctica, *J. Glaciol.*, *54*(188), 881–887.

Galton-Fenzi, B., J. Hunter, R. Coleman, S. Marsland, and R. Warner (2012), Modeling the basal melting and marine ice accretion of the Amery Ice Shelf, *J. Geophys. Res.*, *117*, C09031, doi:10.1029/2012JC008214.

Jacobs, S. S., A. L. Gordon, and J. L. Ardai Jr. (1979), Circulation and melting beneath the Ross Ice Shelf, *Science*, *203*, 439–443, doi:10.1126/science.203.4379.439.

Jacobs, S. S., A. Jenkins, C. F. Giulivi, and P. Dutrieux (2011), Stronger ocean circulation and increased melting under Pine Island Glacier Ice Shelf, *Nat. Geosci.*, *4*, 519–523, doi:10.1038/ngeo1188.

Lewis, E., and R. Perkin (1986), Ice pumps and their rates, *J. Geophys. Res.*, *91*(C10), 11,756–11,762.

Morgan, V. (1972), Oxygen isotope evidence for bottom freezing on the Amery Ice Shelf, *Nature*, *238*(5364), 393–394.

Morgan, V., and W. Budd (1975), Radio-echo sounding of the Lambert Glacier Basin, *J. Glaciol.*, *15*(73), 103–111.

Nicholls, K. W. (1996), Temperature variability beneath Ronne Ice Shelf, Antarctica, from thermistor cables, *J. Geophys. Res.*, *101*(C1), 1199–1210.

Nicholls, K. W., and A. Jenkins (1993), Temperature and salinity beneath Ronne Ice Shelf, Antarctica, *J. Geophys. Res.*, *98*(C12), 22,553–22,568, doi:10.1029/93JC02601.

Nicholls, K. W., and K. Makinson (1998), Ocean circulation beneath the western Ronne Ice Shelf, as derived from in situ measurements of water currents and properties, *Antarct. Res. Ser.*, *75*, 301–318.

Nicholls, K. W., S. Østerhus, K. Makinson, T. Gammelsrød, and E. Fahrbach (2009), Ice-ocean processes over the continental shelf of the southern Weddell Sea, Antarctica: A review, *Rev. Geophys.*, *47*, RG3003, doi:10.1029/2007RG000250.

Nøst, O., and A. Foldvik (1994), A model of ice shelf-ocean interaction with application to the Filcher-Ronne and Ross Ice Shelves, *J. Geophys. Res.*, *99*(C7), 14,243–14,254.

Nunes Vaz, R. A., and G. W. Lennon (1996), Physical oceanography of the Prydz Bay region of Antarctic waters, *Deep Sea Res., Part I*, *43*(5), 603–641.

Pingree, R. D. (1972), Mixing in the deep stratified ocean, *Deep Sea Res. Oceanogr. Abstr.*, *19*, 549–561.

Pritchard, H., S. Ligtenberg, H. Fricker, D. Vaughan, M. Van den Broeke, and L. Padman (2012), Antarctic ice-sheet loss driven by basal melting of ice shelves, *Nature*, *484*(7395), 502–505, doi:10.1038/nature10968.

Raup, B., T. Scambos, and T. Haran (2005), Topography of streaklines on an Antarctic ice shelf from photoclinometry applied to a single advanced land imager (ALI) image, *IEEE Trans. Geosci. Remote Sens.*, *43*(4), 736–742, doi:10.1109/TGRS.2005.843953.

Rignot, E., and S. S. Jacobs (2002), Rapid bottom melting widespread near Antarctic ice sheet grounding lines, *Science*, *296*(5575), 2020–2023.

Scambos, T. A., J. Bohlander, C. Shuman, and P. Skvarca (2004), Glacier acceleration and thinning after ice shelf collapse in the Larsen B embayment, Antarctica, *Geophys. Res. Lett.*, *31*, L18402, doi:10.1029/2004GL020670.

Smedsrud, L. H., and A. Jenkins (2004), Frazil ice formation in an ice shelf water plume, *J. Geophys. Res.*, *109*, C03025, doi:10.1029/2003JC001851.

Smith, N. R., D. Zhaoqian, K. R. Kerry, and S. Wright (1984), Water masses and circulation in the region of Prydz Bay, Antarctica, *Deep Sea Res., Part A*, *31*(9), 1121–1147.

Tison, J., D. Ronveaux, and R. Lorrain (1993), Low salinity frazil ice generation at the base of a small Antarctic ice shelf, *Antarct. Sci.*, *5*(3), 309–322.

Wen, J., Y. Wang, W. Wang, K. Jezek, H. Liu, and I. Allison (2010), Basal melting and freezing under the Amery Ice Shelf, east Antarctica, *J. Glaciol.*, *56*(195), 81–90.

Williams, G., N. Bindoff, S. Marsland, and S. Rintoul (2008), Formation and export of dense shelf water from the Adélie Depression, east Antarctica, *J. Geophys. Res.*, *113*, C04039, doi:10.1029/2007JC004346.

Whitworth, T., A. H. Orsi, S. J. Kim, W. D. Nowlin Jr, and R. A. Locarnini (1998), Water masses and mixing near the Antarctic Slope Front, *Antarctic Research Series*, *75*, 1–27.